Superconducting qubit manipulated by fast pulses: experimental observation of distinct decoherence regimes

2012 New J. Phys. 14 023031

(http://iopscience.iop.org/1367-2630/14/2/023031)

New Journal of Physics
The open-access journal for physics

Superconducting qubit manipulated by fast pulses: experimental observation of distinct decoherence regimes

F Chiarello[1,4], E Paladino[2], M G Castellano[1], C Cosmelli[3], A D'Arrigo[2], G Torrioli[1] and G Falci[2]

[1] Istituto di Fotonica e Nanotecnologie—CNR, Via Cineto Romano 42, 00156 Roma, Italy
[2] Dipartimento di Fisica e Astronomia, Università di Catania and CNR IMM MATIS, Catania, c/o Viale Andrea Doria 6, Ed.10, 95125 Catania, Italy
[3] Dip. Fisica Università 'Sapienza', 00185 Roma, Italy
E-mail: chiarello@ifn.cnr.it

New Journal of Physics **14** (2012) 023031 (16pp)
Received 7 October 2011
Published 14 February 2012
Online at http://www.njp.org/
doi:10.1088/1367-2630/14/2/023031

Abstract. A particular superconducting quantum interference device (SQUID) qubit, namely the double SQUID qubit, can be manipulated by rapidly modifying its potential with the application of fast flux pulses. In this system we observe coherent oscillations exhibiting non-exponential decay, indicating an unconventional decoherence mechanism. Moreover, via tuning the qubit in different conditions (different oscillation frequencies) by changing the pulse height, we observe a crossover between two distinct decoherence regimes and the existence of an 'optimal' point where the qubit is only weakly sensitive to intrinsic noise. We find that this behavior is in agreement with a model considering the decoherence caused essentially by low-frequency noise contributions, and we discuss the experimental results and possible issues.

[4] Author to whom any correspondence should be addressed.

Contents

1. Introduction

In the last decade, superconducting devices have proved to be promising candidates for the implementation of quantum computing [1–3]. Single superconducting qubits [4–7], and simple quantum gates [8] have been realized and tested using different schemes and solutions with impressive results, providing at the same time a unique framework for the study and understanding of intimate aspects of quantum mechanics [9–12]. In order to further improve superconducting qubit performance and overcome the actual limitations, it is fundamental to defeat decoherence due to the variety of solid-state noise sources. The first step in this direction is to identify which are the most detrimental in each specific implementation scheme. This problem has been amply investigated in recent years. The first generation of superconducting qubits [4] were severely affected by low-frequency fluctuations of control variables of different physical origins. Considerable improvement has been achieved by operating the systems at working points naturally protected from low-frequency fluctuations [6, 13] or by new architectures implementing schemes of cavity quantum electrodynamics (QED) in the solid state, the so-called circuit-QED schemes [7, 14]. Research along these lines also requires the consideration of innovative materials [15, 16].

In this paper, we consider a particular superconducting qubit, the double superconducting quantum interference device (SQUID) tunable qubit [17, 18], which, in analogy with the four-junction flux qubit presented in [19], has a tunable gap obtained by replacing a single junction with a dc SQUID. In our case we use an Nb device with a simpler structure (a two-junction SQUID), and the coherent oscillations between flux states are obtained by simply applying fast flux pulses (with respect to the typical qubit time scales) in the absence of applied microwaves pulses [20–22]. Here we report measurements of coherent oscillations at different frequencies obtained by acting on the bias conditions, in particular by modifying the pulse height. Interestingly, modifying the oscillation frequency also affects its decay time, and in particular the shape of the decay envelope. With increasing oscillation frequency, a crossover between two distinct decoherence regimes is observed: an exponential quadratic decay followed by an algebraic behavior. In this last regime, a working point of minimal decoherence is identified. The existence of two decoherence regimes can be explained considering a model system including low-frequency fluctuations of the qubit bias and intrinsic parameters. In particular the existence of an optimal point of reduced sensitivity to the defocusing processes is

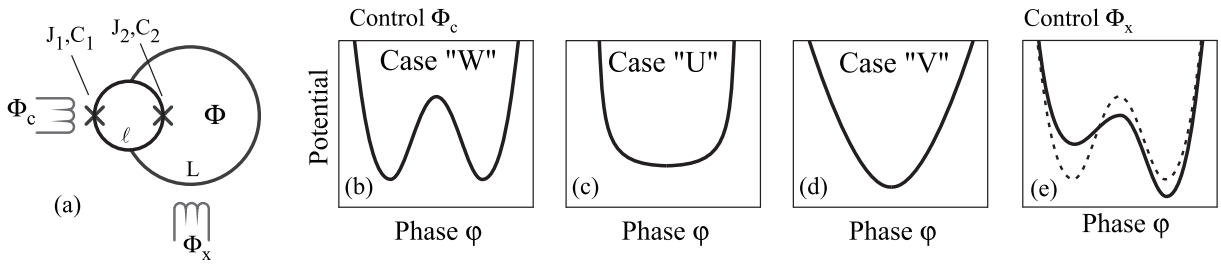

Figure 1. (a) The double SQUID scheme. (b–d) The modification of the potential shape by changing the bias flux Φ_c applied to the small loop. (e) The modification of the potential symmetry by changing the bias flux Φ_x applied to the large loop.

predicted. Our analysis also suggests the possible existence of additional low-frequency noise sources not included in our model.

The paper is organized as follows. In section 2, the double SQUID qubit and its manipulation with flux pulses are described. The experimental measurements of the coherent oscillations are reported in section 3, where we also discuss which phase of the manipulation is expected to be more severely influenced by noise sources. In section 4 we introduce a theoretical model of decoherence processes during the manipulation phase of the experiment and predict the existence of optimal points in the present setup. The fit of the experimental data is reported in section 5 and we present the conclusions in the final section 6.

2. The double SQUID qubit manipulated by fast pulses

The double SQUID qubit consists of a superconducting loop of inductance L interrupted by a dc-SQUID, which is a second superconducting loop of smaller inductance l interrupted by two Josephson junctions with critical currents $J_{1,2}$ and capacitances $C_{1,2}$ (figure 1(a)). In our case it is $L = 85\,\mathrm{pH}$, $l = 7\,\mathrm{pH}$, and the junctions are almost identical, $J_1 \approx J_2 \equiv I_0 = 8\,\mu\mathrm{A}$ and $C_1 \approx C_2 = C/2 = 0.4\,\mathrm{pF}$, with $(J_1 - J_2)/(J_1 + J_2) \approx 2\%$. The two loops are biased by two distinct magnetic fluxes, denoted as Φ_x for the large loop and Φ_c for the small one. When $l \ll L$ the system is approximately described by a Hamiltonian with a single degree of freedom, the total magnetic flux Φ threading the large loop or, equivalently, the phase difference across the dc-SQUID $\varphi = \Phi/\Phi_b$ (where $\Phi_b = \Phi_0/(2\pi) = \hbar/(2\mathrm{e})$ is the reduced flux quantum). The Hamiltonian is the sum of a kinetic contribution $T = -E_C/2\partial_{\varphi\varphi}$ ($E_C = (2e)^2/C$ is the charging energy, and $\partial_{\varphi\varphi}$ stands for the second derivative with respect to the phase) and of the potential

$$U(\varphi) = E_L \left[\frac{(\varphi - \varphi_x)^2}{2} - \beta(\varphi_c) \cos\varphi \right], \tag{1}$$

where $\varphi_x = \Phi_x/\Phi_b$ and $\varphi_c = \Phi_c/\Phi_b$ are the reduced bias fluxes, $\beta(\varphi_c) = \beta_0 \cos(\varphi_c/2)$ is the tuning parameter controlled by φ_c, $\beta_0 = 2I_0L/\Phi_b = E_J/E_L$ and $E_L = \Phi_b^2/L$, $E_J = 2I_0\Phi_b$ are, respectively, the inductive and the Josephson energy. In our case it is $E_C/h = 0.22\,\mathrm{GHz}$, $E_L/h = 1920\,\mathrm{GHz}$ and $E_J/h = 7940\,\mathrm{GHz}$ leading to $\beta_0 = 4.1$. Depending on the value of $\beta(\varphi_c)$, the potential $U(\varphi)$ has a single-well or a double-well shape, with φ_c controlling the barrier height in the double well (figure 1(b)) and the concavity in the single-well case (figures 1(c) and (d)), and φ_x controlling the potential symmetry (figure 1(e)) [23, 24]. The

described potential presents a periodic behaviour in Φ_x and Φ_c [20]. In our case, the working region is such that $\Phi_x \approx 0$ and $\beta(\varphi_c)$ is negative.

In the quasi-symmetric condition ($|\varphi_x| \ll 1$), fundamental to our scheme, we distinguish three important regimes.

- **'W' potential** (figure 1(b)): for $\beta(\varphi_c) < -1$ the potential $U(\varphi)$ has a double-well shape (labeled 'W' for graphical similarity with this shape), with two minima at $\varphi^{\pm}_{\min}$ given by the solutions of the implicit equation $\varphi^{\pm}_{\min} + \beta(\varphi_c)\sin(\varphi^{\pm}_{\min}) = \varphi_x$ and distant $\Delta\varphi = \varphi^{+}_{\min} - \varphi^{-}_{\min}$. For $\varphi_x = 0$ (perfect symmetry) the system is degenerate and energy levels are arranged in doublets. In practical cases, even a small asymmetry $|\varphi_x| \ll 1$ removes the degeneracy still maintaining the doublet structure, with the first two energy levels very close to each other but far away from the upper levels (for example, if $\beta(\varphi_c) = -1.1$ it is sufficient to have $|\Phi_x| > 10^{-9}\Phi_0$ in order to remove the degeneracy). In this case the first two energy eigenstates ($|0\rangle$ and $|1\rangle$) are flux states in the left and right wells ($|L\rangle$ and $|R\rangle$). The energy gap $\hbar\varepsilon = E_L\,\Delta\varphi\,\varphi_x$ between them is almost constant in a large range of values of $\beta(\varphi_c)$ because of the weak dependence of $\Delta\varphi$ on $\beta(\varphi_c)$. Approximate analytical expressions for the important quantities related to this case have been reported in [24].
- **'V' potential** (figure 1(d)): for $\beta(\varphi_c) > -1$, $U(\varphi)$ displays a single well ('V' is used for graphical similarity with this shape), and the system can be approximated by a harmonic oscillator with level spacing given by

$$\hbar\Omega \sim \hbar\Omega_0\sqrt{1+\beta(\varphi_c) - \frac{\beta(\varphi_c)}{[1+\beta(\varphi_c)]^2}\frac{\varphi_x^2}{2}}, \tag{2}$$

  where $\Omega_0 = 1/\sqrt{LC}$.
- **'U' potential** (figure 1(c)): for $\beta(\varphi_c) \approx -1$ we have a rapid transition between the double well (W) and the single well (V) case, passing through a quartic potential (again 'U' is used for graphical similarity with this quartic potential shape). This case is particularly interesting for its strong anharmonicity [25].

The various shapes of the potential $U(\varphi)$ and the possibility of easily passing from one regime to the other are the fundamental features allowing us to use this system as a qubit. For example, the qubit 'rest state' can be realized when the potential takes the quite symmetric double-well shape (W). In this regime the magnetic flux states $|L\rangle$ and $|R\rangle$ are used as computational states. Qubit manipulations can be performed via flux pulses modifying the potential shape, without employing microwave pulses. For example, the initial flux state of the qubit can be prepared by strongly unbalancing the potential in order to obtain just a single minimum (left or right, according to the unbalancing direction), then waiting the necessary time for the complete relaxation in this well and finally returning in the double-well condition. A coherent rotation between flux states (corresponding to an X rotation in the Bloch sphere) can be realized by applying a fast flux pulse on the control φ_c in order to change the potential from the double-well 'W' to the single-well 'V' case ('W–U–V' transition), then waiting in this condition ('V') for a time t and finally returning back ('V–U–W' transition) to the initial double-well case ('W') where the measurement can be carried out. Details of the procedure have been reported in [20, 21].

Here we summarize the main steps of the manipulation. During the rapid 'W-U-V' passage, in particular near the 'U' case, a non-adiabatic transition occurs from the degeneracy point

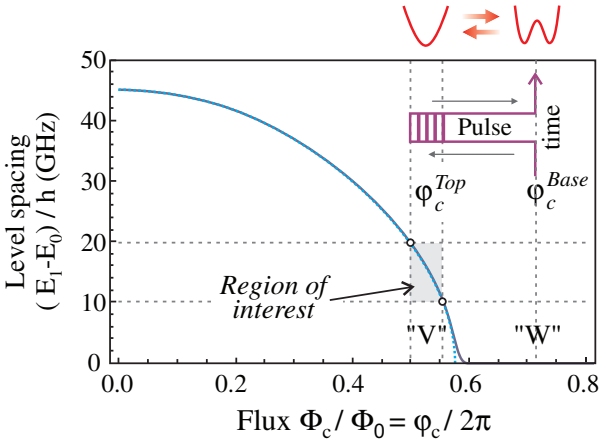

Figure 2. Energy level splitting in h units (continuous blue line) and frequency $\Omega/2\pi$ given by equation (2) (dotted cyan line, almost superimposed on the blue line) for $\varphi_x = 0$ as a function of $\varphi_c = 2\pi\,\Phi_c/\Phi_0$. The dashed horizontal lines mark the range of oscillation frequencies observed (about 10–20 GHz), corresponding to the range of used top values of the applied pulse (defined by the vertical dashed lines). In the inset the flux pulse used for the qubit manipulation is sketched, changing the potential from the two-well 'W' case to the single-well 'V' case (in red).

(in the 'W' case) to the large gap case (in the 'V' condition), corresponding to a partial Landau–Zener transition (see figure 2), which equally populates the first two energy eigenstates in the 'V' harmonic potential with an initial phase depending on the initial qubit state. Only the first two levels will be populated despite the fact that the final potential 'V' is harmonic. In fact, all the transitions occur in the strongly anharmonic case 'U', where transitions to unwanted upper levels can be avoided by accurately choosing the transition speed. During the time t spent in the 'V' potential, a further phase difference $\Delta\theta = \Omega t$ between the two states is acquired. During a final 'V–U–W' passage a second partial Landau–Zener transition specular to the first one (inset of figure 2) will map the total phase into the probability amplitude for the two flux states. For example, if we start the manipulation from an initial left state we will obtain, at the end, the state $|\psi\rangle = \cos(\Omega t/2)|L\rangle + \sin(\Omega t/2)|R\rangle$. The rotation frequency Ω is related to the concavity of the potential in the single-well case, and it is modulated by the top value of the pulse φ_c^{Top} according to equation (2). It corresponds to the energy difference between the first two eigenstates in units of $\hbar$. The readout of the final qubit flux state is performed by a flux discriminator, typically by observing the switching of an unshunted dc-SQUID inductively coupled to the large loop of the qubit [26].

3. Experimental results

In order to realize the described operation experimentally, we need a preparation–manipulation–readout sequence. The initialization in one of the two flux states (left or right) is obtained by applying a control flux Φ_x that strongly unbalances the potential removing one of the two wells. After a time that is sufficient for complete relaxation in the remaining well

(5 μs in our case), the system is brought back to the 'W' condition with a high barrier preserving the prepared state. The modification must be slow enough to avoid unwanted transitions to upper levels, but at the same time it must be fast enough to avoid a final equal population of the two wells; in other words it must be non-adiabatic with respect to the first two levels and adiabatic with respect to the upper ones. Thanks to the final high barrier (which gives a very small gap between the first two levels), this is possible for a very large range of modification time scales (from seconds to tens of nanoseconds). In our case we modify the potential in about 1 μs. Then a flux pulse is applied on φ_c presenting a base value $\varphi_c^{\mathrm{Base}}$, which maintains the qubit potential in the 'W' condition, and a pulse top φ_c^{Top}, which moves the qubit to the 'V' condition only for the duration t of the pulse. At last the final state is read out by using the dc-SQUID discriminator. The preparation–manipulation–readout sequence lasts 100 μs in our measurement, and it is repeated N times (with $N = 100$–10000, according to the required accuracy) in order to estimate the final probability after the manipulation. The sequence is repeated for different pulse durations t in order to reconstruct the oscillation of the final probability. Finally, we repeat the measurement for different top flux pulse values φ_c^{Top}. In order to satisfy the condition $\beta(\varphi_c^{\mathrm{Top}}) > -1$, the flux φ_c^{Top} is varied in the interval $[0.98\,\pi, 1.12\,\pi]$. For the sake of clarity we report in figure 2 the dependence of Ω on φ_c^{Top}. The measurements are carried out in a dilution refrigerator at 30 mK, on a device based on standard Hypres Nb/AlOx/Nb trilayer technology, closed in a system protected by a series of copper, steel and mu-metal shields. The dc bias lines are filtered by different LCL low-pass filters and by thermocoax [27] stages, and attenuators are placed on the fast control lines at different temperature stages (see [20, 21] for further details of the manipulation and of the setup).

If the system is prepared in the $|L\rangle$ state, the probability of measuring the qubit in the same state after the coherent evolution during a time t in the 'V' phase, in the ideal case of no noise sources, reads $P_{LL}(t) = [1 + \cos(\Omega t)]/2$. In figure 3, we report some experimental values of $P_{LL}(t)$ obtained for different pulse heights φ_c^{Top}, implying different oscillation frequencies (indicated in each panel)[5].

Remarkably, changing the pulse height not only modifies the oscillation frequency but also influences qualitatively and quantitatively its decay law. This is more clearly pointed out considering the envelope of each probability, shown in figure 4. In contrast with the exponential decay typically originating from quantum noise, the decay of the probabilities is fitted by the decay law (blue lines in figure 4) [29]:

$$\mathrm{d}(t) = \frac{1}{[1 + (\gamma_{\mathrm{II}} t)^2]^{1/4}} \exp\left[-\frac{(\gamma_{\mathrm{I}} t)^2}{2}\right], \tag{3}$$

with independent fitting parameters, γ_{I} and γ_{II}.

The combination of exponential quadratic and algebraic decay is characteristic of defocusing processes due to fluctuations with the $1/f$ spectrum of the parameters entering the splitting Ω [29, 30]. Similar behaviors have in fact been observed in different architectures and in the presence of microwave manipulation pulses [30]. The observed decay laws therefore suggest that the present experiment is mainly affected by $1/f$ noise in the control fluxes and in the junctions' critical currents. Relaxation processes, typically leading to exponential decay, seem to be weakly effective.

The experimentally estimated values of γ_{I} as a function of the frequency $f = f_0\sqrt{1 + \beta(\varphi_c)}$ ($f_0 = \Omega_0/(2\pi)$) are reported in figure 5 (left panel—red dots). We observe a regular behavior

[5] Similar results have also been obtained by another group in a quite different system [28].

IOP Institute of Physics DEUTSCHE PHYSIKALISCHE GESELLSCHAFT

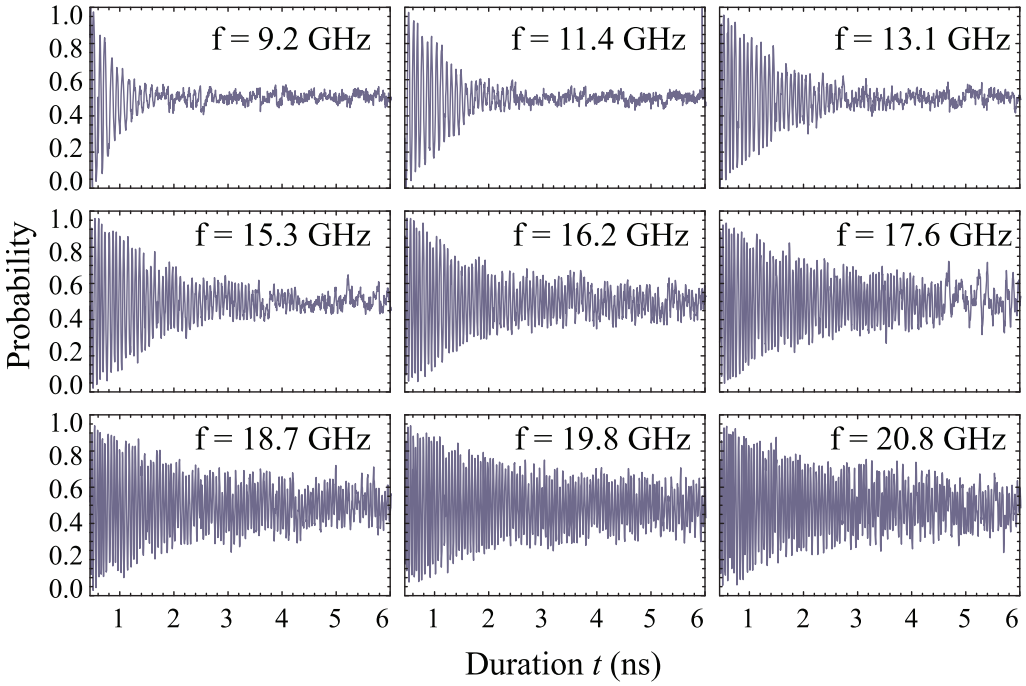

Figure 3. Experimental oscillations of the probability of observing a left state, obtained for different pulse heights. The measured frequency is indicated in the top right part of each plot.

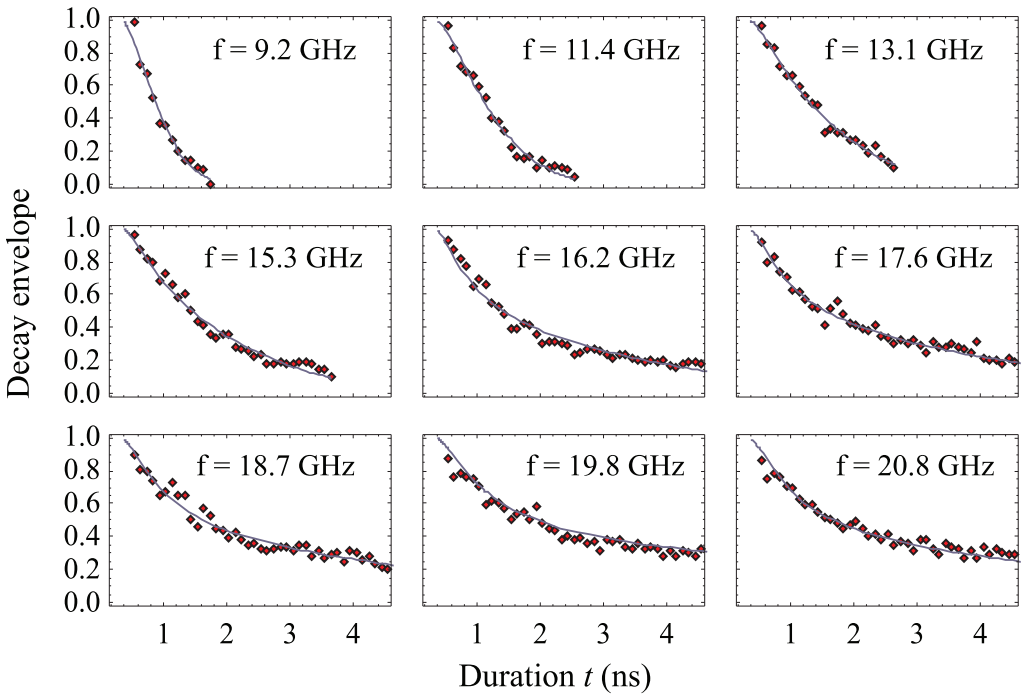

Figure 4. Decay envelopes of the observed oscillations (red points) and relative fitting curves (blue continuous lines).

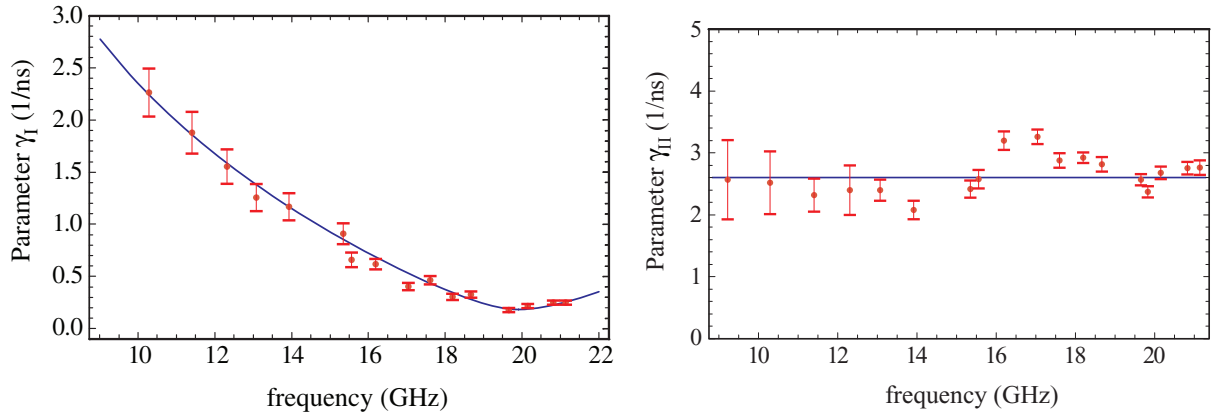

Figure 5. The red points are the decay rates γ_I (left panel) and γ_{II} (right panel) obtained by fitting the experimental decay curves in figure 4 with equation (3). The blue line in the left panel is the fit of the data points with equation (10) (section 4). In the right panel the blue line is the average value of the scattered values of γ_{II}.

characterized by a minimum at $f_0 = \Omega_0/(2\pi) = 19.8\,\text{GHz}$ ($\varphi_c^{\text{Top}} \approx \pi$). This behavior suggests the existence of an optimal point in the present setup. The values of γ_{II}, shown in figure 5 (right panel—red dots), are instead quite scattered and we observe $\gamma_{II} > \gamma_I$, except for frequencies around 10 GHz where $\gamma_{II} \approx \gamma_I$. As a consequence, by changing the operating point, φ_c^{Top}, the probability turns from a decay approximately exponential to an algebraic behavior for frequencies f close to f_0, where γ_I is minimum, highlighting a crossover between two distinct regimes.

In order to further investigate whether this is an appropriate picture, in the following section we theoretically analyze the effects of low- and high-frequency flux and critical current noise in the present setup. Before proceeding with the analysis, we need to identify the phases of the manipulation which are presumably more severely affected by noise sources. The various parts of the manipulation protocol described in section 2 can be discussed separately as follows.

1. **Initial phase 'W':** during the initial 'W' phase, when the barrier is very high and the system is rigorously prepared in one of the two states, any possible transition between wells is blocked by the high barrier. The system remains in an eigenstate to high accuracy.
2. **'W–U–V' transition:** the effect of noise during this rapid transition is a very difficult problem, involving out-of-equilibrium dynamics. However, for the present experiment, noise during this phase is presumably irrelevant. In fact, any noise source acting during this transition should affect the oscillation amplitude independently of the pulse duration. Therefore we expect that it merely produces a net reduction in the visibility of the oscillation at the start time. Since we are able to observe oscillations with high visibilities, up to 95% (figure 2), we conclude that the effect of noise during this phase is small. This fact can be tentatively explained by considering that the critical region where the change of the potential shape occurs ('U' region) is crossed over in a very short time (of the order of picoseconds), shorter than the typical time of coupling with the environment (a few nanoseconds).

3. **Phase 'V':** on the contrary, relaxation and decoherence will act heavily during the single-well condition 'V', with an effect depending on the time t of permanence in this phase.
4. **'V–U–W' transition:** for the return transition from the single- to the double-well potential ('V-U-W'), the same considerations of the 'W–U–V' transition hold (based on the initial visibility of the oscillation), so that one can conclude that in this case the effect of noise is also rather small.
5. **Final phase 'W':** finally, when the barrier is raised again in the final condition before the readout ('W'), transitions between the two wells are again blocked by the barrier. In this case the final state will be a superposition of the left/right states and the effect of dephasing can be quite strong. However, since we are just interested in the final population of one of the localized states, the information on the relative phase between the two states can be disregarded.

In conclusion, we expect that the observed decay of the probability can be attributed mainly to noise sources acting during phase 'V', when the system evolves during time t and several repetitions of the protocol are performed. In the following section we will investigate the effect of low-frequency noise during repeated measurement protocols in the 'V' phase of the present experiment.

4. Defocusing during repeated measurements

Superconducting qubits in the various implementations are usually affected by broadband and non-monotonic noise [6, 30, 31]. The various noise sources responsible for this phenomenology have qualitatively different influences on the system evolution. To solve the qubit dissipative dynamics we apply the multi-stage elimination approach introduced in [29]. In the simplest cases the effect of noise with large spectral components at low frequencies (adiabatic noise), like $1/f$ noise, and the effect of noise acting at frequencies of the order of the qubit splitting (quantum noise), can be treated independently. The leading effect of adiabatic noise during repeated measurement protocols is defocusing, analogous to inhomogeneous broadening in nuclear magnetic resonance (NMR) [32]. It is expressed by the 'static path' or static noise approximation (SPA) describing the average of signals oscillating at randomly distributed effective frequencies [29, 30]. Defocusing can be sensitively reduced by operating at 'optimal points' where the variance of the stochastic frequency is minimal [33]. Quantum noise is instead responsible for relaxation processes. It can be treated by solving a Bloch–Redfield master equation, which leads to exponential decay both of the populations, with relaxation time denoted by T_1 in the NMR notation, and of the coherences with the decoherence time $T_2 = 2T_1$ [35].

The measurements reported in the previous section indicate a dominant adiabatic noise. Here we focus our attention on the effect of noise during the single-well 'V' phase, when the harmonic approximation holds with level spacing given in equation (2). Defocusing originates from variations of the effective frequency Ω in the different measurement runs that we attribute to fluctuations of the control bias fluxes $\delta\varphi_x$, $\delta\varphi_c$ and of the critical current δI_0, which correspond to fluctuations of β_0, $\delta\beta_0$. Fluctuations of the magnetic fluxes are caused by extrinsic and intrinsic sources. The electromagnetic circuit originates from quantum noise. In addition, electric lines used to bias the qubit, in particular those coming from the room-temperature electronics, are responsible for noise components mainly at low frequencies, where the filtering is weakly effective (below tens of kHz). The intrinsic flux noise acting on the superconducting

loops is typically $1/f$ (adiabatic). Different models of flux noise microscopic sources have been proposed, such as electron hopping between traps either with fixed randomly oriented spins [36] or with spin flips [37]. Spin diffusion along the superconducting surface has also been proposed [38]. Fluctuations of the critical current are instead due only to intrinsic causes, such as the presence of two state fluctuators in the junction barrier [15, 39]. In the present article, we do not address the important issue of the microscopic source of the fluctuations. Rather, we note the existence of low-frequency variations of the effective oscillation frequency and describe their effects in the adiabatic approximation. To this end we assume small fluctuations of Ω given in equation (2) around the nominal values of the control parameters, φ_c^{Top} and $\varphi_x = 0$. The expansion of Ω to second order in the fluctuations leads to $\Omega + \delta\Omega$, where

$$\frac{\delta\Omega}{\Omega_0} \sim b_1\,\delta\beta_0 + c_1\,\delta\varphi_c - \frac{1}{2}[a_2\,\delta\varphi_x^2 + b_2\,\delta\beta_0^2 + c_2\,\delta\varphi_c^2 + m_2\,\delta\varphi_c\delta\beta_0]. \tag{4}$$

The coefficients of the first- and second-order terms are (for simplicity here we use φ_c for φ_c^{Top})

$$b_1 = \frac{1}{2}\frac{\cos(\varphi_c/2)}{\sqrt{1+\beta(\varphi_c)}}, \quad c_1 = -\frac{1}{4}\frac{\beta_0\sin(\varphi_c/2)}{\sqrt{1+\beta(\varphi_c)}} \tag{5}$$

and

$$a_2 = \frac{\beta(\varphi_c)}{2(1+\beta(\varphi_c))^{5/2}}, \quad b_2 = \frac{\cos^2(\varphi_c/2)}{4(1+\beta(\varphi_c))^{3/2}}, \tag{6}$$

$$c_2 = \frac{1}{8\sqrt{1+\beta(\varphi_c)}}\left(\beta(\varphi_c) + \frac{\beta_0^2\sin^2(\varphi_c/2)}{2(1+\beta(\varphi_c))}\right), \quad m_2 = \frac{\sin(\varphi_c/2)}{2(1+\beta(\varphi_c))^{3/2}}\left(1 + \frac{\beta(\varphi_c)}{2}\right). \tag{7}$$

In the SPA the off-diagonal elements of the qubit reduced density matrix (RDM), $\rho(t)$, on the basis of the lowest eigenstates in the 'V' potential $\{|0\rangle, |1\rangle\}$, are obtained by evaluating the average over the fluctuations $\delta\varphi_x$, $\delta\varphi_c$ and δ_{β_0}

$$\langle\rho_{01}(t)\rangle = \rho_{01}(0)\,\mathrm{e}^{-\mathrm{i}\Omega t}\,\langle\mathrm{e}^{-\mathrm{i}\delta\Omega t}\rangle, \tag{8}$$

where we assume that fluxes and critical current fluctuations are uncorrelated random variables with Gaussian distribution, zero mean and standard deviations σ_x, σ_c and σ_{β_0}, respectively. We remark that for the fluctuations of the critical current this assumption should be checked considering the microscopic source of the I_0 fluctuations. The power spectra of the control flux biases and of the critical current measured in similar flux or phase qubits reveal a $1/f$ behavior at low frequencies [36, 39]. The variance of the corresponding variables, σ_α^2 ($\alpha = x, c, \beta_0$), is proportional to the amplitude of the $1/f$ spectrum, $S_\alpha^{1/f}(\omega) = \pi\sigma_\alpha^2[ln(\gamma_{M\alpha}/\gamma_{m\alpha})\,\omega]^{-1}$ ($\gamma_{m\alpha}$ and $\gamma_{M\alpha}$ are the low- and the high-frequency cut-offs of the $1/f$ region).

In order to compare with the experiments, we evaluate the average probability $\langle P_{LL}(t)\rangle$. For the chosen initial condition, $|\psi(t=0)\rangle = |L\rangle = (|0\rangle + |1\rangle)/\sqrt{2}$ the probability reads $\langle P_{LL}(t)\rangle = \frac{1}{2} + \langle\mathrm{Re}[\rho_{01}(t)]\rangle$. Where we assumed that the sum of the populations of the lowest eigenstates of the harmonic potential is constant, $\rho_{00}(t) + \rho_{11}(t) = 1$. This assumption is justified in the adiabatic approximation, where populations do not evolve. It also holds in the presence of quantum noise, provided leakage from the bi-dimensional Hilbert space can be neglected. The averaged probability thus reads

$$\langle P_{LL}(t)\rangle = \frac{1}{2}[1 + \langle\cos((\Omega+\delta\Omega)t)\rangle] = \frac{1}{2}[1 + \mathrm{d}(t)\cos(\Omega t + \theta)], \tag{9}$$

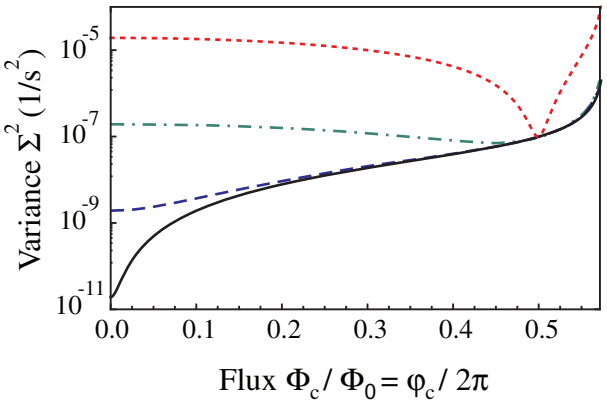

Figure 6. Variance of Ω given by equation (13) as a function of φ_c in the allowed interval of values where $\beta(\varphi_c) > -1$ for $\sigma_c \sim \sigma_x \approx 3 \times 10^{-4}$, and different σ_{β_0} values 2×10^{-5}, 2×10^{-4}, 2×10^{-3} and 2×10^{-2} from the bottom to the top.

where $\mathrm{d}(t) = |\langle \exp \mathrm{i}\delta\Omega t\rangle|$ and $\theta = \arg[\langle \exp \mathrm{i}\delta\Omega t\rangle]$. The coherence $\langle \rho_{01}(t)\rangle$ in the SPA is obtained by evaluating the average equation (8) with $\delta\Omega$ given by equation (4). For short times (neglecting contributions $\propto t^4$ with respect to terms $\propto t^2$) $\mathrm{d}(t)$ is indeed given by equation (3) with γ_{I} and γ_{II} given by

$$\gamma_{\mathrm{I}} = \Omega_0 \sqrt{b_1^2 \sigma_{\beta_0}^2 + c_1^2 \sigma_c^2}, \tag{10}$$

$$\gamma_{\mathrm{II}} = \Omega_0 \sqrt{b_2^2 \sigma_{\beta_0}^4 + c_2^2 \sigma_c^4 + a_2^2 \sigma_x^4 + m_2^2 \sigma_{\beta_0}^2 \sigma_c^2}. \tag{11}$$

Note that the first-order terms of the expansion (4) enter γ_{I} and the second-order terms enter γ_{II}. Finally, we include the possibility of incoherent energy exchanges with the environment due to quantum noise. In the simplest version of the multi-stage elimination approach the overall decay factor of the coherence is

$$\mathrm{d}(t) = |\langle \exp \mathrm{i}\delta\Omega t\rangle|\, \mathrm{e}^{-t/T_2}, \tag{12}$$

where the decoherence time due to quantum noise, T_2, depends on the power spectrum of the flux and of the critical current fluctuations at frequency Ω.

The existence of an optimal point in the present setup depends on the possibility of minimizing the standard deviation of the effective splitting Ω, $\Sigma = \sqrt{\langle \delta\Omega^2\rangle - \langle \delta\Omega\rangle^2}$ [33, 34]. In fact, from the short-time expansion of equation (8) we find that $|\langle \mathrm{e}^{-\mathrm{i}\delta\Omega t}\rangle| \approx 1 - (\Sigma t)^2/2$, thus defocusing is reduced when Σ is minimal. In the present case, from (4), we find that

$$\Sigma^2 = \gamma_{\mathrm{I}}^2 + \frac{1}{2}\gamma_{\mathrm{II}}^2. \tag{13}$$

Because of the periodicity of the first-order terms in (4), included in the coefficients b_1 and c_1 defined in equation (5), Σ is minimal either at $\varphi_c \approx 0$, when $\sigma_c > \sigma_{\beta_0}$, or at $\varphi_c \approx \pi$ in the opposite case. This is illustrated in figure 6 where we show Σ for typical values of the variances σ_c and σ_x [36, 39] and increasing values of σ_{β_0}. Depending on which condition applies to a specific setup, the device can be operated at the proper optimal point[6].

[6] Note that at the optimal point the first derivative of the splitting Ω with respect to either φ_c or β_0 is non-vanishing. It is not possible to reach an optimal point of vanishing differential dispersion as for charge [6] or flux qubits [13].

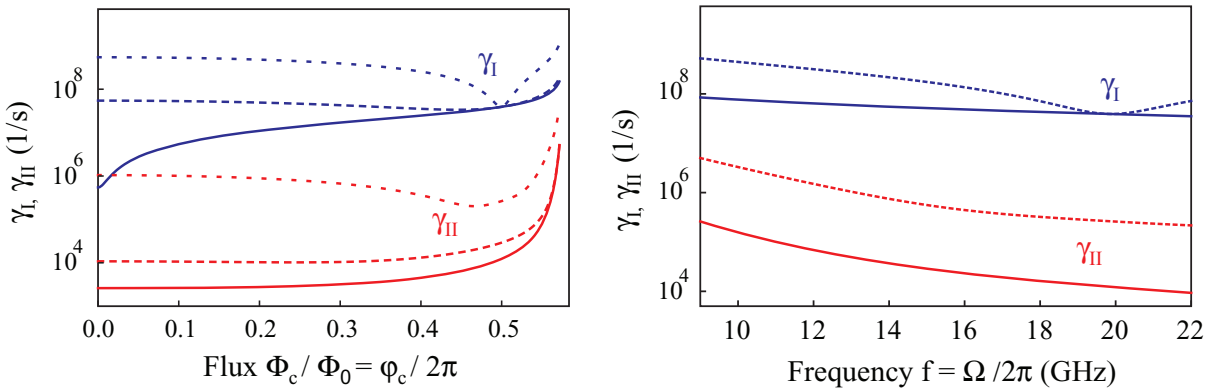

Figure 7. Left panel: $\gamma_{\rm I}$ (blue) and $\gamma_{\rm II}$ (red) as a function of φ_c for $\sigma_c \sim \sigma_x \approx 3 \times 10^{-4}$, and different σ_{β_0} values (solid lines for 2×10^{-5}, dashed lines for 2×10^{-3} and dotted lines for 2×10^{-2}). Right panel: $\gamma_{\rm I}$ (blue) and $\gamma_{\rm II}$ (red) as a function of $f = \Omega/2\pi$ in the experimental regime $\varphi_c \in [0.98\,\pi, 1.2\,\pi]$ for the previous values of σ_c, σ_x and $\sigma_{\beta_0} = 2 \times 10^{-5}$ (solid line) and $\sigma_{\beta_0} = 2 \times 10^{-2}$ (dotted line).

The dependence of $\gamma_{\rm I}$ and $\gamma_{\rm II}$ on the operating point is reported in figure 7 for the same parameters of figure 6. In the considered regime, $\gamma_{\rm I}$ is minimal at the optimal point, wherever it is located (left panel). This is a consequence of the fact that under these conditions the variance of Ω is dominated by the first-order terms and $\Sigma \approx \gamma_{\rm I}$. In the right panel of figure 7 we show $\gamma_{\rm I}$ and $\gamma_{\rm II}$ as a function of the frequency f when φ_c varies in the experimental range around $\varphi_c \approx \pi$ (as indicated in figure 2). In this frequency range $\gamma_{\rm I}$ is minimal only when $\sigma_{\beta_0} > \sigma_c$ (corresponding to the dashed and dotted curves in figure 6). We may thus expect that a similar situation occurs in the present experiment, with an optimal point at $\varphi_c^{\rm Top} \approx \pi$ corresponding to a minimum of $\gamma_{\rm I}$. However, we note that for the parameters in figure 7, since $\gamma_{\rm I} > \gamma_{\rm II}$, the coherence decay $\mathrm{d}(t)$ is dominated by the exponential factor $\exp(\gamma_{\rm I}^2 t^2/2)$, *independently* of the optimal point location. Since in the present experiment we observe a crossover from an exponential to an algebraic decay by changing the working point, for some operating conditions around $\varphi_c^{\rm Top} \approx \pi$ it should turn out that $\gamma_{\rm I} \lesssim \gamma_{\rm II}$. Since at the considered working point ($\varphi_x = 0$), fluctuations of the flux φ_x contribute to the second-order in (4), the above relation between $\gamma_{\rm I}$ and $\gamma_{\rm II}$ may in principle occur when the flux variances differ considerably. Such a situation is, however, unlikely; the dependence of $1/f$ flux noise on the SQUID size as due to a 'global magnetic field noise' has in fact been ruled out [36]. Such a situation is also excluded in the present experiment. An illustrative case with $\sigma_x \gg \sigma_c$ is shown in figure 8. Due to the increased weight of the second-order terms in (4), $\gamma_{\rm II}$ has a local minimum at the optimal point, $\varphi_c^{\rm Top} \approx \pi$. However, for frequencies close to the minimum, being $\gamma_{\rm II} < \gamma_{\rm I}$, the decay factor would be exponential rather than algebraic, in contrast to the observations reported in the previous section.

We conclude from this analysis that the present model, considering the adiabatic fluctuations of the two fluxes φ_c and φ_x, and of the critical current, predicts the existence of an optimal point of minimal variance of the effective splitting and of minimal $\gamma_{\rm I}$, when first-order terms in the expansion of the effective frequency Ω dominate. On the other side, it is difficult to predict the simultaneous existence of an optimal point at $\varphi_c^{\rm Top} \approx \pi$ where $\gamma_{\rm I}$ is minimum *and* $\gamma_{\rm I} < \gamma_{\rm II}$ is only close to the minimum, as observed in figure 5. A plausible scenario is

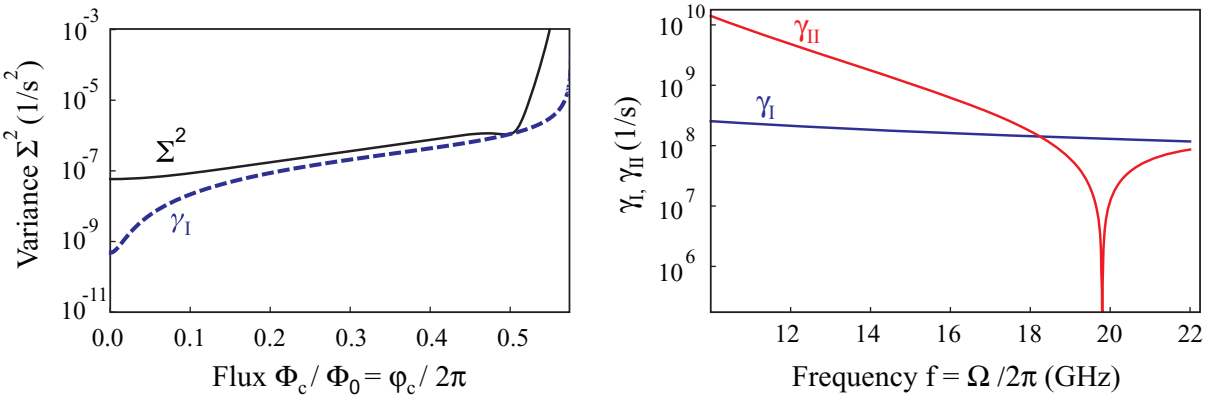

Figure 8. Left panel: the variance Σ^2 as a function of φ_c with the minimum at $\approx \pi$; the continuous line represents (13); the dashed line is the first-order approximation $\Sigma \approx \gamma_{\mathrm{I}}$. Right panel: the rates γ_{I} and γ_{II} as a function of f. The variances in this example have been fixed to highlight the regime $\gamma_{\mathrm{I}} \gtrsim \gamma_{\mathrm{II}}$, and are $\sigma_c \approx 10^{-3}$, $\sigma_x \approx 10^{-1}$, $\sigma_{\beta_0} \approx 10^{-4}$.

that the present experiment is sensitive to first-order contributions, entering equation (10) for γ_{I}, whereas second-order effects entering γ_{II}, equation (11), are masked possibly by additional noise sources not included in our analysis. For instance, our model does not include SQUID inductance fluctuations with the $1/f$ power spectrum, which are highly correlated to $1/f$ flux noise [40].

5. Fit of the experimental data: γ_{I}, γ_{II}

According to the analysis of the previous section, whereas for γ_{I} we may expect agreement between equation (10) and the experimental data, we expect that equation (11) for γ_{II} has to be supplemented by an additional contribution of different origin. Therefore, in order to extract γ_{I}, γ_{II} and $1/T_2$ from the experimental data we fit the envelopes of the experimental curves in figure 3, considering them as *independent* parameters.

Indeed, the experimentally estimated γ_{I} for the different oscillation frequencies f can be fitted with equation (10), giving remarkable agreement with fitting parameters $\sigma_c = 1.4 \times 10^{-3}$ and $\sigma_{\beta_0} = 0.105$, corresponding to $\sigma_{\Phi_c} = 223\mu\Phi_0$ and $\sigma_{I_0} = 1.7\,\mu$A, see figure 5 (left panel, blue line). The noise on the flux φ_c, in addition to the $1/f$ behavior, is possibly also influenced by low-frequency noise components due to the room-temperature instrumentation. For the estimated noise variances, fluctuations of the critical current are almost always dominating except for the optimal point at $f_0 = \Omega_0/(2\pi) = 19.8\,\mathrm{GHz}$ where the effect of flux noise emerges. The existence of this optimal point is evident from the decays in figure 4, where a crossover between two decay regimes is observed: a fast decay at lower frequencies is followed by a slower decay at higher frequencies.

On the other side, the value of σ_{β_0} obtained from the fit is much larger than the values reported in other superconducting qubits [36, 39]. An independent check of this quantity in the present setup is not possible, since measurements of the low-frequency power spectrum of critical current noise are not available at present. One possible explanation of the quite high value of σ_{I_0} is related to the materials used for the qubit fabrication. In fact, other

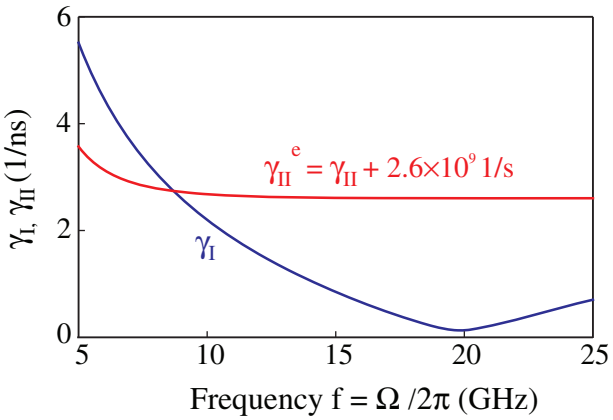

Figure 9. Plot of γ_I (blue) and $\gamma_{II}^e = \gamma_{II} + 2.6 \times 10^9\,s^{-1}$ (red) as a function of f for variances extracted from the fit of γ_I, $\sigma_c \approx \sigma_x \approx 10^{-3}$, $\sigma_{\beta_0} \approx 10^{-1}$.

superconducting qubits based on the same materials and fabrication technology and displaying coherence times similar to those reported in our experiment (a few nanoseconds) [22] presented a considerable enhancement of these times by improving the used materials, for example by introducing SiN_x dielectric films instead of standard SiO_2 for the crossover wiring [15, 16]. A full understanding of this point requires the repetition of the experiment with the use of different materials and technologies. Another possible source of this inconsistency is the assumed Gaussian distribution for the critical current fluctuations, $\delta\beta_0$. Evaluating possible deviations from the Gaussian approximation requires the consideration of a microscopic model of critical current fluctuations. This is another possible extension of the present analysis.

The values of γ_{II} extracted from the fit of the oscillations in figure 3 are scattered around an average value of $\sim 2.6 \times 10^9\,s^{-1}$, as shown in figure 5. Equation (11) for γ_{II} with $\sigma_x \sim \sigma_c = 1.4 \times 10^{-3}$ and $\sigma_{\beta_0} = 0.105$ predicts that $\gamma_{II} \ll \gamma_I$, in contrast with the observations. However, including a constant (frequency-independent) noise contribution in the second-order terms, i.e. defining an effective $\gamma_{II}^e \approx \gamma_{II} + 2.6 \times 10^9\,s^{-1}$, the crossover from exponential to algebraic decay where $\gamma_I \ll \gamma_{II}$, visible in figure 5, can be quantitatively reconstructed, as illustrated in figure 9.

Finally, the reported measurements do not allow for a reliable estimate of the effect of quantum noise, included in the exponential decay term with T_2. The observations are compatible with a decoherence time T_2 with a lower limit of tens of nanoseconds, which is reasonable in these types of qubits [15].

6. Conclusions

In conclusion, we considered the manipulation of a double SQUID qubit by fast flux pulses and observed the decay envelope of the obtained oscillations for different control conditions, corresponding to different oscillation frequencies. The shapes of the decay envelopes show a peculiar behavior with a crossover between two distinct regimes. These behaviors can be attributed to various sources of adiabatic noise affecting the system. The effect of high-frequency noise is negligible, and this indicates a correct filtering and shielding of the system.

We observed a crossover between an exponential and an algebraic decay regime, with an optimal point where the decay is algebraic. We demonstrated that this behavior is due to

the interplay of first-order effects of low-frequency flux and critical current noise. In general, intrinsic fluctuation of the critical current dominates, except at the optimal point where the weaker effect of flux bias fluctuations springs up. The existence of the optimal point is an interesting characteristic for possible applications.

The effect of second-order fluctuating terms is still not well understood and requires further investigation. To this end, we plan to repeat the experiment with different, improved materials. The ensuing noise characterization may possibly provide new insights into the low-frequency noise sources in this kind of setup.

Acknowledgments

This work was supported by the Italian MIUR under the PRIN2008 C3JE43 project and by the EU through grant no. PITN-GA-2009-234970.

References

[1] Ladd T D *et al* 2010 *Nature* **464** 45–53
Buluta I *et al* 2011 *Rep. Prog. Phys.* **74** 104401–17
[2] Clarke J and Wilhelm F K 2008 *Nature* **453** 1031–42
[3] Devoret M H and Martinis J M 2004 *Quantum Inf. Process.* **3** 163–203
[4] Nakamura Y *et al* 1999 *Nature* **398** 786
Yu Y *et al* 2002 *Science* **296** 889
Martinis J M *et al* 2002 *Phys. Rev. Lett.* **89** 117901
Chiorescu I *et al* 2003 *Science* **299** 1869
Yamamoto T *et al* 2003 *Nature* **425** 941
Saito S *et al* 2004 *Phys. Rev. Lett.* **93** 037001
[5] Johansson J *et al* 2006 *Phys. Rev. Lett.* **96** 127006
Deppe F *et al* 2008 *Nat. Phys.* **4** 686
Manucharyan V E *et al* 2009 *Science* **326** 113–6
[6] Vion D *et al* 2002 *Science* **296** 886
[7] Wallraff A *et al* 2004 *Nature* **431** 162–7
[8] Pashkin Yu A *et al* 2003 *Nature* **421** 823
Berkley A J *et al* 2003 *Science* **300** 1548
Yamamoto T *et al* 2003 *Nature* **425** 941
Izmalkov A *et al* 2004 *Phys. Rev. Lett.* **93** 037003
Majer J B *et al* 2005 *Phys. Rev. Lett.* **94** 090501
Plantenberg J H *et al* 2007 *Nature* **447** 836
McDermott R *et al* 2005 *Science* **307** 1299
Steffen M *et al* 2006 *Science* **313** 1423
Hime T *et al* 2006 *Science* **314** 1427
Niskanen A O *et al* 2007 *Science* **316** 723
Majer J *et al* 2007 *Nature* **449** 443
van der Ploeg S H W *et al* 2007 *Phys. Rev. Lett.* **98** 057004
Fay A *et al* 2008 *Phys. Rev. Lett.* **100** 187003
DiCarlo L *et al* 2009 *Nature* **460** 240–4
[9] Johnson B R *et al* 2010 *Nat. Phys.* **6** 663–7
[10] Palacios-Laloy A *et al* 2010 *Nat. Phys.* **6** 442–7
[11] Ansmann M *et al* 2009 *Nature* **461** 504–6

[12] Hofheinz M *et al* 2008 *Nature* **454** 310–4
[13] Yoshihara F *et al* 2006 *Phys. Rev. Lett.* **97** 167001
[14] Blais A *et al* 2004 *Phys. Rev.* A **69** 062320
Devoret M H *et al* 1992 in *Quantum Tunneling in Condensed Media* ed Y Kagan and A J Leggett (Amsterdam: Elsevier) pp 313–45
[15] Martinis J M *et al* 2004 *Phys. Rev. Lett.* **95** 210503
[16] McDermott R 2009 *IEEE Trans. Appl. Supercond.* **19** 2–13
[17] Carelli P *et al* 2001 *IEEE Trans. Appl. Supercond.* **11** 210–4
[18] Chiarello F 2000 *Phys. Lett.* A **277** 189–93
[19] Paauw F G *et al* 2009 *Phys. Rev. Lett.* **102** 090501
[20] Castellano M G *et al* 2010 *New J. Phys.* **12** 043047
[21] Poletto S *et al* 2009 *New J. Phys.* **11** 013009
[22] Poletto S *et al* 2009 *Phys. Scr.* **T137** 014011
[23] Castellano M G *et al* 2007 *Phys. Rev. Lett.* **98** 177002
[24] Chiarello F 2007 *Eur. Phys. J.* B **55** 7–11
[25] Zorin A B and Chiarello F 2009 *Phys. Rev.* B **80** 214535
[26] Castellano M G *et al* 2003 *J. Appl. Phys.* **94** 7935–7
[27] Zorin A B 1995 *Rev. Sci. Instrum.* **66** 4296
[28] Steffen M *et al* 2010 *J. Phys.: Condens. Matter* **22** 053201
[29] Falci G *et al* 2005 *Phys. Rev. Lett.* **94** 167002
Paladino E *et al* 2003 *Physica E: Low-dimensional Systems and Nanostructures* **18** 29
[30] Ithier G *et al* 2005 *Phys. Rev.* B **72** 134519
[31] Astafiev O *et al* 2004 *Phys. Rev. Lett.* **93** 267007
[32] Schlichter C P 1996 *Principles of Magnetic Resonance* (New York: Springer)
[33] Paladino E *et al* 2010 *Phys. Rev.* B **81** 052502
[34] Paladino E *et al* 2011 *New J. Phys.* **13** 093037
[35] Cohen-Tannoudji C, Dupont-Roc J and Grynberg G 1993 *Atom–Photon Interactions* (New York: Wiley-Interscience)
[36] Koch R H *et al* 2007 *Phys. Rev. Lett.* **98** 267003
[37] de Sousa R 2007 *Phys. Rev.* B **76** 245306
[38] Faoro L and Ioffe L B 2008 *Phys. Rev. Lett.* **100** 227005
[39] Van Harlingen D J *et al* 2004 *Phys. Rev.* B **70** 064517
[40] Sendelbach S *et al* 2009 *Phys. Rev. Lett.* **103** 117001